Fast and Accurate Permittivity Estimation Algorithm for UWB Internal Imaging Radar

Ryunosuke Souma, Shouhei Kidera, and Tetsuo Kirimoto
Graduate School of Informatics and Engineering, University of Electro-Communications, Tokyo, Japan
e-mail : souma@secure.ee.uec.ac.jp

***Abstract*—Ultra-wideband (UWB) pulse radar has high-range resolution and permeability in a dielectric medium, and has great promise for non-destructive inspection or early-stage detection of breast cancer. We have already proposed an accurate imaging algorithm for targets in a dielectric medium, which employs the advanced principle of the RPM (Range Points Migration) algorithm. Although this method offers an accurate internal target image, it is based on the ideal assumption that the permittivity of the dielectric medium is completely known. Although there are various permittivity estimation algorithms, they require an enormous amount of computation, or are hardly applicable to an arbitrary dielectric boundary. To tackle this difficulty, we propose a fast permittivity estimation algorithm suitable for arbitrary dielectric boundaries. In particular, this method makes use of the dielectric boundary points and their normal vectors, preliminarily determined by the existing RPM method. Then, the actual time delay in dielectric permeation is calculated from the ranges observed under Snell's law. The calculation time is about 5 sec with a Xeon 3.0 GHz processor. Results from numerical simulation verify that our algorithm estimates permittivity with less than 10% error even in noisy situations.**

***Key words*—UWB pulse radar, Permittivity estimation, Internal imaging, Arbitrary dielectric boundary, Range Points Migration**

I. Introduction

UWB signals were approved for commercial use by the Federal Communications Commission (FCC) in 2002, and have a frequency width of over 500 MHz or a 10 dB fractional bandwidth over 25% [1]. UWB pulses with high-range resolution and dielectric permeability are promising for internal imaging radar systems. As such, they can be used non-destructively to determine the location and shape of a rebar or pipe and detect cavities or cracks within walls [2], and are promising in medicine for detecting breast tumors at an early stage [3]. While various imaging algorithms for these applications have been studied, such as time-reversal algorithm [4] and microwave imaging via space-time beamforming algorithm [3], these algorithms are based on signal integrations, which often require a large computational calculation.

To overcome the above problem, we have already proposed a fast and accurate UWB imaging algorithm for targets buried in a dielectric medium [5]. This algorithm is based on the advanced principle of the RPM (Range Points Migration) algorithm [6] which accurately determines the propagation path in a dielectric medium by exploiting the target boundary points and their normal vectors under Snell's law. Although, this algorithm enhances imaging accuracy and remarkably reduces the computational amount by specifying boundary extraction, it is based on ideal assumption that the permittivity of dielectric medium is uniform and completely known. In actual imaging scene, the permittivity is unknown, and should be estimated from the observed data.

As a solution to this issue, there are various permittivity estimation algorithms based on numerical solutions of domain integral equations [7] or employing time delays and known dielectric structures based on the geometric optics approximation for through-the-wall applications [8]. However, [7] often requires an enormous computation amount for solving the integral equations, or [8] is hardly applicable to an arbitrary dielectric medium boundary because it mostly assumes a known and simple dielectric structure. To make the permittivity estimation more feasible, we proposes a fast and accurate permittivity estimation algorithm suitable for arbitrary dielectric boundaries. In particular, this algorithm makes use of dielectric boundary information that includes the location and normal vector correctly offered by the RPM algorithm. Then, the actual time delay in propagating through the dielectric can be accurately calculated from the observed permeation data. The numerical simulation results show that our method achieves a fast and accurate permittivity estimation with less than 10% error even in noisy situations.

II. System Model

Figure 1 shows the system model. We assume that a target and dielectric medium with uniform permittivity have arbitrary shapes with clear boundaries. The propagation speed c of the radio wave in air is a known constant. Two omni-directional antennas are scanned along the circle with a center $\boldsymbol{r}_c$ and radius R_c that can completely surround a dielectric object as shown in Fig. 1. A mono-cycle pulse is used as the transmitting current. The real space, in which the target and antenna are located, is normalized by the center wavelength λ of the transmitted pulse. One transmitting and receiving antenna is located at $\boldsymbol{r}_{\mathrm{TR}} = (X, Z)$, and an antenna that only receives is located at $\boldsymbol{r}_{\mathrm{R}} = (X, Z)$, where $\boldsymbol{r}_c = (\boldsymbol{r}_{\mathrm{TR}} + \boldsymbol{r}_{\mathrm{R}})/2$ holds. $S_{\mathrm{TR}}(\boldsymbol{r}_{\mathrm{TR}}, R)$ and $S_{\mathrm{R}}(\boldsymbol{r}_R, R)$ are defined as the output of the Wiener filter at antenna positions $\boldsymbol{r}_{\mathrm{TR}}$ and $\boldsymbol{r}_{\mathrm{R}}$, respectively, where $R = \mathrm{c}t/2\lambda$ is expressed by time t, (see Ref. [6] for details). Figure 2 illustrates the examples of $S_{\mathrm{TR}}(\boldsymbol{r}_{\mathrm{TR}}, R)$ and $S_{\mathrm{R}}(\boldsymbol{r}_R, R)$, respectively, where the target and dielectric are assumed.

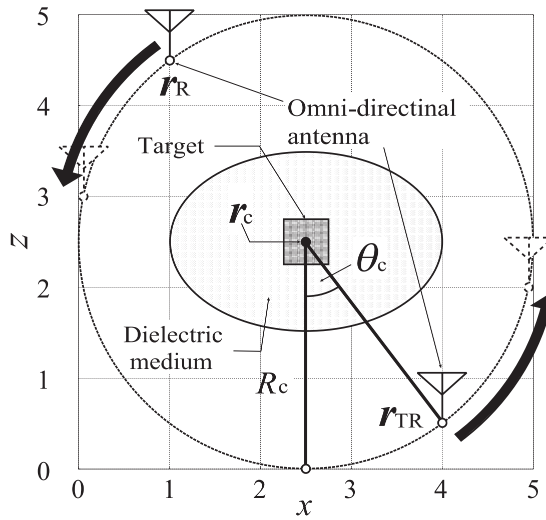

Fig. 1. System model.

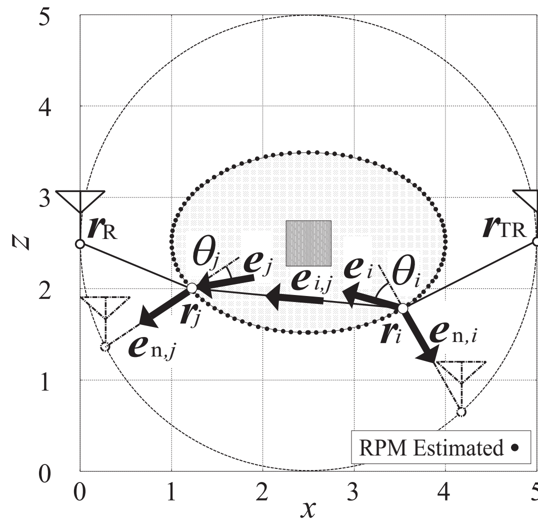

Fig. 3. Target points obtained by RPM and example of propagation path.

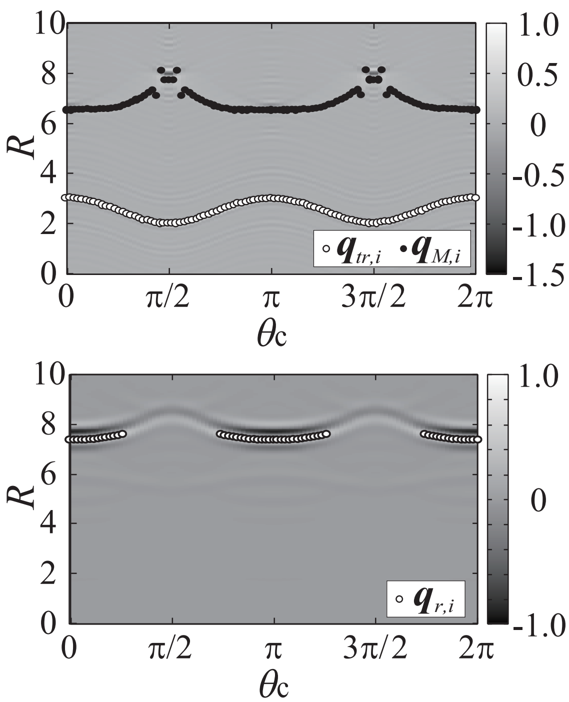

Fig. 2. Outputs of Wiener filter $S_{\mathrm{TR}}\left(\boldsymbol{r}_{\mathrm{TR}}, R\right)$ (upper) and $S_{\mathrm{R}}\left(\boldsymbol{r}_{\mathrm{R}}, R\right)$ (lower).

III. Proposed Method

Various permittivity estimation algorithms have been proposed based on numerical solution of domain integral equation [7] or exploiting the time delay data under rectangular dielectric structures for through-the-wall imaging purpose [8]. However, Each algorithm has an essential problem that [7] basically requires an enormous amount of computation due to recursive solution of the integration equation, and [8] is also difficult to be applied to arbitrary dielectric medium boundary.

To overcome the both problems, we propose a novel permittivity estimation algorithm that is suitable for an arbitrary dielectric boundary. First, this algorithm employs the dielectric boundary points preliminarily produced by an RPM algorithm [6], which achieves extremely accurate imaging employing the extracted range points defined as $\boldsymbol{q}_{tr,i} = (X_{tr,i}, Z_{tr,i}, R_{tr,i}), (i = 1, ..., N_{tr})$. These components are extracted from the local maxima $S_{\mathrm{TR}}(\boldsymbol{r}_{\mathrm{TR}}, R)$. Then, RPM directly converts these range points to the target boundary points as $\boldsymbol{r}_i = (x_i, z_i), (i = 1, ..., N_{tr})$, where one-to-one correspondence is satisfied. A set of these target points is defined as $\mathcal{T}_{\mathrm{rpm}}$. Note that, the normal vector on each target boundary point is calculated without a derivative operation as $\boldsymbol{e}_{\mathrm{n},i} = (X_{tr,i} - x_i, Z_{tr,i} - z_i)/R_{tr,i}$. This algorithm selects the first and second incident points $(\hat{\boldsymbol{r}}_{\mathrm{I}}(\epsilon_t), \hat{\boldsymbol{r}}_{\mathrm{P}}(\epsilon_t))$ on the dielectric boundary according to Snell's law using,

$$(\hat{\boldsymbol{r}}_{\mathrm{I}}(\epsilon_t), \hat{\boldsymbol{r}}_{\mathrm{P}}(\epsilon_t)) = \underset{(\boldsymbol{r}_i, \boldsymbol{r}_j) \in \mathcal{T}_{\mathrm{rpm}}^2}{\arg\min} \{|\boldsymbol{e}_i(\epsilon_t) - \boldsymbol{e}_{i,j}|^2 + |\boldsymbol{e}_j(\epsilon_t) - \boldsymbol{e}_{i,j}|^2\}, \tag{1}$$

where $\boldsymbol{e}_i(\epsilon_t) = \boldsymbol{R}_o(\theta_i(\epsilon_t))(-\boldsymbol{e}_{\mathrm{n},i})$, $\boldsymbol{e}_j(\epsilon_t) = \boldsymbol{R}_o(\theta_j(\epsilon_t))(-\boldsymbol{e}_{\mathrm{n},j})$ and $\boldsymbol{e}_{i,j} = (\boldsymbol{r}_i - \boldsymbol{r}_j)/|\boldsymbol{r}_i - \boldsymbol{r}_j|$. $\boldsymbol{R}_o(\theta)$ is a rotation matrix in the counterclockwise direction, $\theta_i(\epsilon_t)$ and $\theta_j(\epsilon_t)$ denote the refraction angles calculated by Snell's law and the relative permittivity ϵ_t. Figure 3 shows an estimation example of $\hat{\boldsymbol{r}}_{\mathrm{I}}(\epsilon_t)$, $\hat{\boldsymbol{r}}_{\mathrm{P}}(\epsilon_t)$ and estimated dielectric boundary produced by RPM. Then, the propagation distance from $\boldsymbol{r}_{\mathrm{TR}}$ to $\boldsymbol{r}_{\mathrm{R}}$ are calculated:

$$R(\epsilon_t; X_{r,i}, Z_{r,i}) = \frac{1}{2}\Big\{|\hat{\boldsymbol{r}}_{\mathrm{I}}(\epsilon_t) - \boldsymbol{r}_{\mathrm{TR}}| + \sqrt{\epsilon_t}|\hat{\boldsymbol{r}}_{\mathrm{I}}(\epsilon_t) - \hat{\boldsymbol{r}}_{\mathrm{P}}(\epsilon_t)| + |\hat{\boldsymbol{r}}_{\mathrm{P}}(\epsilon_t) - \boldsymbol{r}_{\mathrm{R}}|\Big\}. \tag{2}$$

Next, the permeative range points $\boldsymbol{q}_{r,i} = (X_{r,i}, Z_{r,i}, R_{r,i}), (i = 1, ..., N_r)$ are extracted from the local maxima of $S_{\mathrm{R}}(X, Z, R)$. The relative permittivity for

TABLE I
ESTIMATION ERRORS IN VARIOUS NOISY SITUATIONS.

S/N (dB)	ϵ_t	e_ϵ (%)	$\bar{e}_r$ ($\times 10^{-2}\lambda$)
∞	4.76	4.8	2.17
45	4.74	5.2	2.28
35	4.74	5.2	2.62
25	4.41	8.8	3.44

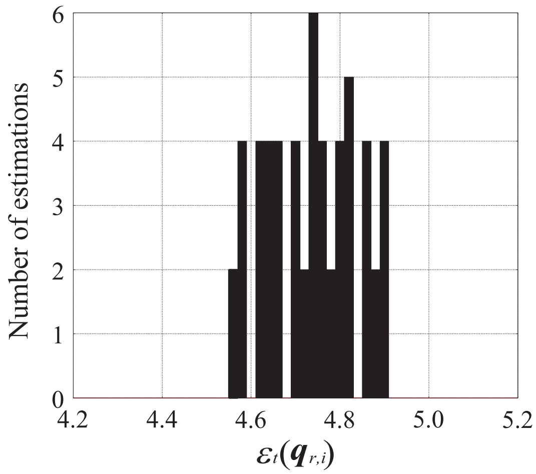

Fig. 4. Histogram of $\epsilon_t\left(\boldsymbol{q}_{r,i}\right)$ in noiseless situation.

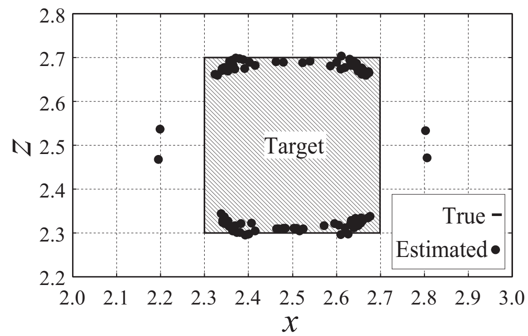

Fig. 5. Estimeted internal image in noiseless situation.

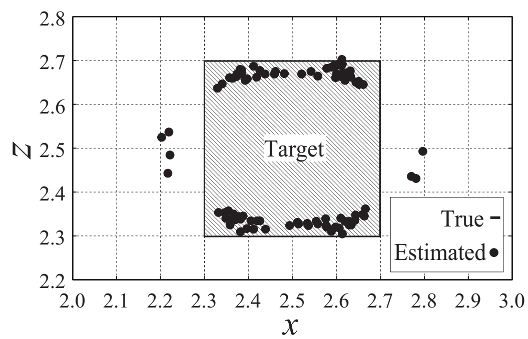

Fig. 6. Estimated internal image at S/N = 25dB.

each range point is determined by

$$\epsilon_t\left(\boldsymbol{q}_{r,i}\right) = \arg\min_{\epsilon_t} |R\left(\epsilon_t : X_{r,i}, Z_{r,i}\right) - R_{r,i}|. \quad (3)$$

Finally, the optimum permittivity $\hat{\epsilon}_t$ is calculated as

$$\hat{\epsilon}_t = \frac{\sum_{\boldsymbol{q}_{r,i}\in Q} S_{\rm R}\left(\boldsymbol{q}_{r,i}\right)\epsilon_t\left(\boldsymbol{q}_{r,i}\right)}{\sum_{\boldsymbol{q}_{r,i}\in Q} S_{\rm R}\left(\boldsymbol{q}_{r,i}\right)}, \quad (4)$$

where $Q = \left\{\boldsymbol{q}_{r,i} \middle| \left|\epsilon_t\left(\boldsymbol{q}_{r,i}\right) - \tilde{\epsilon}_t\right| < \Delta\epsilon_t\right\}$, and $\tilde{\epsilon}_t$ is the mode value calculated by the distribution of $\epsilon_t\left(\boldsymbol{q}_{r,i}\right)$. $\Delta\epsilon_t$ is the threshold to eliminate outliers. This algorithm is applicable to an arbitrary dielectric boundary with a uniform permittivity. It achieves high-speed processing employing only the time delay information that is accurately determined by the boundary points and their normal vectors offered by RPM.

IV. PERFORMANCE EVALUATION IN NUMERICAL SIMULATION

In this section, we evaluate the performance based on FDTD (Finite Difference Time Domain). The conductivity of the target is set to $1.0 \times 10^7 \mathrm{S/m}$. The conductivity and relative permittivity of the dielectric medium are set to $0.01 \mathrm{S/m}$ and $\epsilon_t = 5.0$, respectively. Here, the locations and shapes of the target and dielectric medium are set as in Fig. 1. $\boldsymbol{r}_c = (2.5, 2.5)$, $R_c = 2.5$ are set, and the scanning sample is 101 points with the same interval. Figure 4 shows the histogram of estimated permittivity $\epsilon_t\left(\boldsymbol{q}_{r,i}\right)$ obtained by our algorithm, where the dielectric boundary points produced by RPM are used as shown in Fig. 3. The mode value of $\epsilon_t\left(\boldsymbol{q}_{r,i}\right)$ is obtained with $\tilde{\epsilon}_t = 4.75$, and the optimum relative permittivity calculated in Eq. (4) is $\hat{\epsilon}_t = 4.76$ in this case. The relative error e_ϵ is 4.8%. Furthermore, the computation time of permittivity estimation is less than 5 sec with a Xeon 3.0 GHz processor. Figure 5 shows the estimated target boundary points produced by the former imaging algorithm [5] employing the relative permittivity estimated by our method. While the top and bottom sides of the target can be reconstructed, the left and right sides of the boundary fall into shadow. This is because the range points around both sides of the target are not retrieved due to a distorted propagation path depending on the dielectric boundary. Moreover, there are some inaccurate points around the target edges, which we think are caused by the scattered waveform deformation.

In addition, we investigate the noisy situation. The white Gaussian noise is added to $S_{\rm TR}(X, Z, R)$ and $S_{\rm R}(X, Z, R)$, where the signal-to-noise ratio (S/N) is defined as the ratio of the peak instantaneous signal power to the average noise power after applying the matched filter. The numerical simulation results for the noiseless case and the cases S/N = 45 dB, 35 dB, and 25 dB are summarized in Table I, where $\bar{e}_r$ is defined as mean value of $e_r\left(\boldsymbol{q}_{M,i}\right)$ shown in Eq. (5). Figure 6 shows the estimated target boundary points for S/N = 25 dB.

Moreover, for the quantitative analysis, the evaluation value is introduced as

$$e_r\left(\boldsymbol{q}_{M,i}\right) = \min_{\boldsymbol{r}_{\rm true}} \left|\left|\boldsymbol{r}_M\left(\boldsymbol{q}_{M,i}\right) - \boldsymbol{r}_{\rm true}\right|\right|, \quad (5)$$

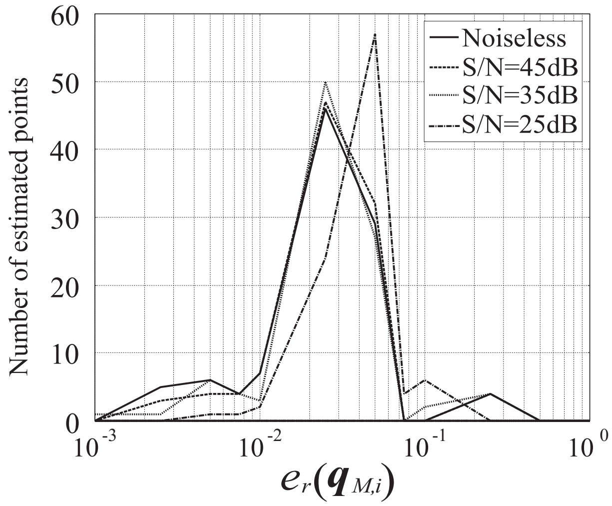

Fig. 7. Number of estimated points error in each $e_r\left(\boldsymbol{q}_{M,i}\right)$ at noiseless and noisy cases.

where $\boldsymbol{q}_{M,i}$ expresses the range points extracted from the second local maximum $S_{\rm TR}(\boldsymbol{r}_{\rm TR}, R)$ as shown in Fig. 2, $\boldsymbol{r}_{\rm true}$ is the location of the true target points, and $\boldsymbol{r}_M\left(\boldsymbol{q}_{M,i}\right)$ expresses estimated internal target points created by the method [5]. Figure 7 shows the error in the number of estimated target points for each $e_r\left(\boldsymbol{q}_{M,i}\right)$ in all situations. This figure shows that the mean error for target boundary extraction is less than $0.05\ \lambda$ for all situation where S/N $\geq$ 25 dB. However, Table I shows that our method has a small estimation error even for higher S/N. The reason for this error is that our method is based on the geometric optics approximation, and does not consider the scattered waveform deformation that causes small errors in range extraction. In our future work, this issue will be treated with a recursive approach based on waveform estimation and imaging processes, to enhance the accuracy of permittivity estimation.

V. Conclusion

We proposed a novel permittivity estimation algorithm for a dielectric medium with an arbitrary shape boundary, where the dielectric boundary points and their normal vectors obtained by RPM are effectively used based on Snellfs law. This algorithm has two significant advantages: One is that it does not require a recursive approach to solving an integral equation, resulting in lower computation, and the other is that it is applicable to an arbitrary dielectric boundary shape, so that it is nonparametric for imaging. In numerical simulation based on FDTD, our algorithm reduce errors in relative permittivity estimation to less than 10 % even for S/N = 25 dB and the calculation time is about 5 sec with a Xeon 3.0 GHz processor. As a result, the internal image obtained employing the exiting technique [5] offers a target boundary with an accuracy on the order of 1/100 wavelength accuracy.

References

[1] R. J. Fontana, “Recent System Applications of Short-Pulse Ultra-Wideband (UWB) Technology,” *IEEE Trans. Microwave Theory Tech.*, vol. 52., no. 9, pp. 2087-2103, Sep. 2004.

[2] A. Boryssenko, O. Boryssenko, A. Lishchenko, and V. Prokhorenko, “Inspection of Internal Structure of Walls by Subsurface Radar,” *IEEE AerospaceandElectronicSystemsMagazine*, pp. 28-31, Oct. 2006.

[3] Xu Li, Essex J. Bond, Barry D. Van Veen, and Susan C. Hagness, “An overview of Ultra-Wideband Microwave Imaging via Space-Time Beamforming for Early-Stage Breast-Cancer Detection,” *IEEE Antennas Propagat. Mag.*, vol. 47, No. 2, pp. 19-34, Feb., 2005.

[4] Panagiotis Kosmas, and Carey M. Rappaport, “A Matched-Filter FDTD-Based Time Reversal Approach for Microwave Breast Cancer Detection,” *IEEE Trans. Antennas Propagat.*, vol. 54, No. 4, pp. 1257-1264, Apr., 2006.

[5] K. Akune, S. Kidera, and T. Kirimoto, “Fast and Accurate Imaging Algorithm for Targets in Dielectric Medium for UWB Radars,” *IEICE Gen. Conf*. C-1-32, Mar., 2011(in Japanese).

[6] S. Kidera, T. Sakamoto, and T. Sato, “Accurate UWB Radar Three-Dimensional Imaging Algorithm for a Complex Boundary Without Range Point Connections,” *IEEE Trans. Geosci. & Remote Sens.*, vol. 48, no. 7, pp. 1993-2004, Apr., 2010.

[7] A. Franchois and C. Pichot, “Microwave Imaging-Complex Permittivity Reconstruction with a Levenberg-Marquardt Method,” *IEEE Trans. Antennas. Propagat.*, vol. 45, no. 2, pp. 203-215, Feb., 1997.

[8] J. Ren, Y. Zhang, T. Jiang, and W. Chen, “Analysis of signal propagation path modeling of UWB Through-the-wall Radar,” *IEEE Asia Pacific Microwave Conference*, pp. 1076-1079, 2009.